SUPERSONIC TURBULENT FLOW MODELLING OVER LARGE AMPLITUDE-TO-WAVELENGTH PERIODIC WAVY SURFACES

by

LIM WEI FONG

Thesis submitted in fulfilment of the requirements for the

Bachelor Degree of Engineering (Honours) (Aerospace Engineering)

July 2021

ENDORSEMENT

I, Lim Wei Fong hereby declare that all corrections and comments made by the supervisor and examiner have been taken consideration and rectified accordingly.

Wei Fong

(Signature of Student)

Date: 12 July 2021

Sarjit

(Signature of Supervisor)

Name: Dr Sarjit Singh Sidhu Junior

Date: 27 June 2021

(Signature of Examiner)

Name: Dr Ahmad Zulfaa Mohamed Kassim

Date: 12 July 2021

DECLARATION

This thesis is the results of my own investigation, except where otherwise stated and has not previously been accepted in substance for any degree and is not being concurrently submitted in candidature for any other degree.

Wei Fong

(Signature of Student)

Date: 27 June 2021

ACKNOWLEDGEMENT

First and foremost, I would like to express my heartfelt gratitude to my final year project supervisor, Dr. Sarjit Singh Sidhu Junior, for clarifying my doubts on the theories and providing insightful comments on the simulation works and writing of this thesis with his professional engineering perspectives. He also prepared guidance on using software such as Pointwise and Tecplot 360 to shorten the software training period efficiently.

I also would like to offer my special thanks to School of Aerospace Engineering, Universiti Sains Malaysia, for delivering all the facilities required to accomplish this project, such as the computers in the CATIA lab and the ANSYS software package. Moreover, I am grateful to Mrs. Rahayu bt.Dorahim@Abdul Rahim who always provides her technical support and assistance on restoring the remote connection between my laptop and the computers in the lab.

Furthermore, I want to thank my coursemate, Mr. Lee Kah Kheng, who is also under the supervision of Dr. Sarjit Singh Sidhu Junior. He always issues me his supports physically and mentally and initiates small discussions among us to share the knowledge learned from the literature and the experiences of using the software.

SUPERSONIC TURBULENT FLOW MODELLING OVER LARGE AMPLITUDE-TO-WAVELENGTH PERIODIC WAVY SURFACES

ABSTRACT

Due to ablation by the high enthalpy flow accelerated by the nozzle, various surface roughness patterns are formed on the post ablated inner wall's surface of the nozzle. These surface roughness patterns will induce disturbances to the supersonic flow and may lead to flow separation, which contributes to the rise of the total drag, followed by reduced thrust output. In the present study, the surface roughness pattern focused is the cross-hatched pattern, which is modelled into a simplified 2-D model of roughness elements in the form of periodically repeating wavy surfaces by using SolidWorks. A numerical experiment is conducted by using ANSYS Fluent to investigate the effect of a larger amplitude-to-wavelength ratio of wavy wall surface on the flow field properties and corresponding drag induced. Moreover, to study the characteristics of the supersonic flow field over a 2-D periodic wavy surface under overexpanded flow conditions using CFD. Parameter to be manipulated for different amplitude-to-wavelength ratios is the surface wavelengths and keeping the wave amplitudes constant at 0.375 mm. The steady-state simulations will be run for 14 variants with amplitude-to-wavelength ratios of wavy surfaces (0.008-0.057) under overexpanded conditions and a freestream Mach number of 3.2 by using k-omega SST turbulence model. The number of oblique shock waves and expansion waves is found to increase with the decreasing of surface wavelengths in the general flow features. Due to the presence of the shockwaves in all cases, the total drag force is always pressure-dominated, and the pressure contribution increases with the substantial reduction of surface wavelengths.

SUPERSONIC TURBULENT FLOW MODELLING OVER LARGE AMPLITUDE-TO-WAVELENGTH PERIODIC WAVY SURFACES

ABSTRAK

Pelbagai corak kekasaran yang terbentuk pada permukaan dinding dalaman muncung adalah disebabkan oleh ablasi oleh aliran entalpi tinggi yang dipercepatkan oleh muncung. Corak kekasaran permukaan ini akan menyebabkan gangguan kepada aliran supersonik dan boleh menyebabkan pemisahan aliran, yang menyumbang kepada peningkatan jumlah seretan, diikuti dengan pengurangan tujahan keluaran. Dalam kajian ini, corak kekasaran permukaan yang difokuskan ialah corak menetas silang yang dimodelkan untuk menjadi model elemen kekasaran 2-D yang dipermudahkan dalam bentuk permukaan bergelombang berulang secara berkala dengan menggunakan SolidWorks. Eksperimen berangka dilakukan untuk menyiasat kesan nisbah amplitud-ke-panjang gelombang permukaan dinding bergelombang yang lebih besar kepada sifat medan aliran dan seretan dengan menggunakan ANSYS Fluent. Lebih-lebih lagi, tujuan yang kedua adalah untuk mengkaji ciri-ciri medan aliran supersonik di atas permukaan bergelombang berkala 2-D di bawah keadaan ekspansi berlebihan dengan menggunakan CFD. Parameter yang akan dimanipulasikan untuk berbagai-bagai nisbah amplitud-ke-panjang gelombang adalah panjang gelombang permukaan dan memastikan amplitud gelombang tetap pada 0.375 mm. Simulasi keadaan mantap akan dijalankan untuk 14 variasi yang berbeza dalam nisbah amplitud-ke-panjang gelombang permukaan bergelombang (0.008-0.057) dalam keadaan ekspansi berlebihan dan Mach freestream sebanyak 3.2 dengan menggunakan model turbulensi SST k-omega. Bilangan gelombang kejutan serong dan gelombang pengembangan didapati meningkat dengan penurunan

panjang gelombang permukaan dalam ciri aliran umum. Oleh kerana adanya gelombang kejutan dalam semua kes, jumlah daya seret selalu dikuasai oleh tekanan, dan sumbangan tekanan meningkat dengan pengurangan panjang gelombang permukaan secara substansial.

TABLE OF CONTENTS

LIST OF FIGURES

LIST OF TABLES

LIST OF ABBREVIATIONS

2-D	: Two Dimensional
3-D	: Three Dimensional
CD	: Converging-Diverging
CAD	: Computer-Aided Design
CFD	: Computational Fluid Dynamics
GIT	: Grid Independence Test
RANS	: Reynolds Averaged Navier-Stokes
SST	: Menter’s Shear Stress Transport
AUSM	: Advection Upstream Splitting Method
PGX	: Pressure Gradient in the X-direction
OSW	: Oblique Shock Wave
EW	: Expansion Wave
CW	: Compression Wave
SWBLI	: Shock-Wave/Boundary-Layer Interaction
FP	: Flat Plate

LIST OF SYMBOLS

a	: speed of sound
A	: surface amplitude
A^*	: nozzle throat cross-sectional area
A_e	: nozzle exit cross-sectional area
C_f	: skin friction coefficient
d^*	: diameter of the critical cross-section of the circular nozzle
d_e	: diameter of the exit cross-section of the circular nozzle
h	: thickness of the plate
h^*	: height of the flat nozzle throat
h_e	: height of the flat nozzle exit
k	: turbulent kinetic energy
l	: displacement of the roughness contour
L	: length of the plate
$\dot{m}$	: mass flow rate
M_t	: compressibility function
P_e	: nozzle exit pressure
q	: ratio of the nozzle throat area to the nozzle exit area
r	: radius of the local section of nozzle

R	: gas constant
Re	: Reynold's number
Re_x	: Reynold's number at a distance x
S	: effective temperature/Sutherland's constant
T	: static temperature
T_0	: reference temperature
u_τ	: friction velocity at the nearest wall
U_∞	: free stream velocity
V	: velocity of the fluid
V_e	: nozzle exit velocity
x	: length of the fluid
y	: absolute distance to the nearest wall
y^+	: dimensionless wall distance
α	: angle of sharp leading edge with respect to the centre line
γ	: ideal gas constant
ρ	: density of the fluid
μ	: dynamic viscosity
μ_0	: reference value of viscosity
λ	: surface wavelength
v	: local kinematic viscosity of the fluid

ω	: specific dissipation rate
τ_w	: wall shear stress
τ_{jk}	: stress tensor
$\alpha^*{}_{\infty}$	: model constant
α_{∞}	: model constant
$\beta^*{}_{\infty}$	: model constant
ζ^*	: model constant
M_{t0}	: model constant
a_1	: model constant
$\beta_{i,1}$	: model constant
$\beta_{i,2}$	: model constant
$\sigma_{k,1}$	: model constant
$\sigma_{k,2}$	: model constant
$\sigma_{\omega,1}$	: model constant
$\sigma_{\omega,2}$	: model constant

CHAPTER 1

INTRODUCTION

1.1 Overview

Launch vehicles operate under changing atmospheric pressure due to different altitudes. However, the fixed geometric ratio of the nozzle allows the launch vehicle to achieve its optimum performance at a certain altitude only. Figure 1.1 displays RD-180 rocket engine with dual nozzle design and the geometric ratio of which is fixed. The exit flow of the nozzle is under-expanded if the operating altitude is above the optimal altitude. Conversely, the output flow of the nozzle is under an overexpanded condition if the operating altitude is below the optimal height. Either under-expansion or overexpansion will lead to an undesirable outcome to the nozzle, which is the loss of thrust. Due to the under-expansion of jet flow, the loss of thrust ranges from 7% to 9% (Semenov et al., 2016). A solution to this problem, especially at higher altitudes is to use higher altitude nozzle attachment which would compensate the loss of thrust expected at altitude. However, in order the beneficially make use these effects, the nozzle attachments need to be strong enough to withstand the high temperature combustion products of the nozzle yet light enough. A solution to this is to make use of composite materials. Figure 1.2 depicts the dual nozzle with nozzle attachment. Also, composite materials are prone to ablation, with roughness elements forming on the smooth walls of the nozzle walls which will inevitably effects thrust levels due to inherent wave drag.

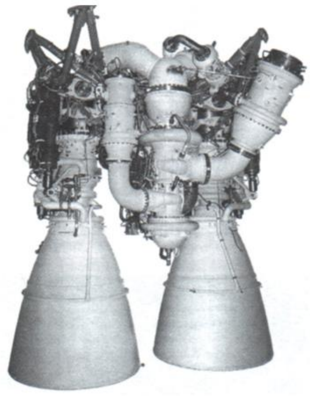

Figure 1.1: RD-180 rocket engine with dual nozzle design

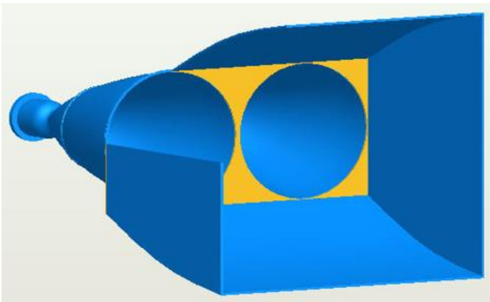

Figure 1.2: Dual nozzle with nozzle attachment

1.2 Problem Statement

Eventually, the high enthalpy exhaust gas which is accelerated by the nozzle will ablate the surface of the nozzle's inner wall. The post ablated surface contains various kinds of surface roughness patterns, including the cross-hatched patterns which is the topic of this research. These surface roughness elements will induce additional drag and thus degrading the rocket nozzle performance by reducing the thrust output and specific impulse. The question of how much of the beneficial effects of using a nozzle attachment at altitude is reduced by the formation of roughness elements due to ablation is addressed in this work.

1.3 Motivation

The geometry of the surface roughness implemented in this research is a 2-D wavy surface as it is more realistically represents the complex profile of the post ablated rocket nozzle's inner walls' surface. The investigations on the effect of wavy surface on the flow behaviour were only carried out numerically under subsonic and supersonic flow conditions in the past studies. There is one numerical study conducted by C. J. Tyson and N. D. Sandham who investigated the effect of a 2-D periodic wavy surface on the supersonic flow field, flow properties, and the drag force, which is quite close to this research, but the variations of the surface wavelengths they studied are only three and the turbulence model they implemented is not practicable in the present work. Worth noting that for supersonic freestream conditions, the compressibility effects, affects the flow field, where changes are highly non-linear depending on various parameters including the those of the roughness elements and the freestream conditions. Therefore, CFD simulations will be conducted over 14 variants of amplitude-to-wavelength ratios of the wavy surface, which are mainly manipulated by the surface wavelengths and keeping the amplitude constant, by utilizing RANS turbulence model which is practicable to study the effect of these variants on the supersonic flow field for this research work.

1.4 Research Objectives

This research is carried out with two objectives, which are:

- To study the characteristics of the supersonic flow field over a 2-D periodic wavy surface under overexpanded flow conditions using CFD.
- To investigate the effect of a larger amplitude-to-wavelength ratio of a wavy wall surface on the flow field properties and the corresponding rise in total drag.

1.5 Thesis Outline

For the outline of this research, this thesis is composed of five chapters, namely Introduction, Literature Review, Methodology, Results and Discussions, and Conclusions and Recommendations.

Chapter 1 briefly introduces the nozzle and its interaction with the extremely hot flow and describes the problem statements, motivation to this research, research objectives, and thesis outline. Chapter 2 demonstrates the review on the past experimental and numerical works conducted which are strongly correlated to the surface roughness patterns. Chapter 3 details the CFD processes, which are pre-processing, solution and postprocessing, and GIT. Chapter 4 displays and discusses the qualitative and quantitative results on the supersonic flow field and flow properties extracted from the simulation files employing postprocessing software. Chapter 5 concludes the findings analysed from Chapter 4 and provides some recommendations for future research.

CHAPTER 2

LITERATURE REVIEW

2.1 Formation of Cross-Hatched Patterns

Due to ablation from high enthalpy supersonic flow, different kinds of surface roughness patterns could be imprinted on the inner surface of nozzle walls which highly depends on the flow structure. One of these surface roughness patterns with diamond shape is studied in this research, which is named as cross-hatched patterns because this pattern could lead to adverse effects, such as augmentation of the associated smooth wall heating rate in terms of heat transfer (Swigart, 1974) and has the largest effect in inducing roll moment as compared to longitudinal grooves and turbulent wedges surface patterns in terms of body dynamics (McDevitt, 1971). The appearances of cross-hatched surface roughness patterns are shown in Figure 2.1 and Figure 2.2.

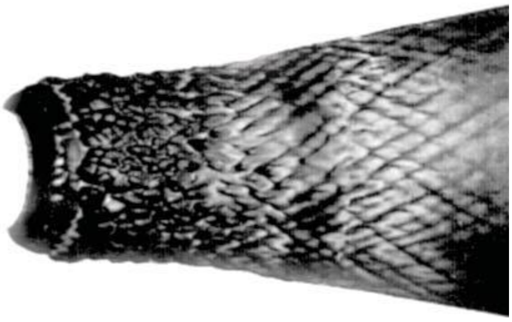

Figure 2.1: Cross-hatched pattern in the diverging section of a nozzle (Kochetkov, 2013)

Figure 2.2: Cross-hatched pattern in the inner nozzle wall's surface (Kochetkov, 2018)

A few flow conditions are required to be fulfilled for the cross-hatched surface roughness pattern to form. Larson and Mateer conducted the experiments on steel-tipped Lucite cones of different cone angles in the NASA Ames 3.5-ft Hypersonic Wind Tunnel at Mach 7.4, and determined that a local supersonic flow is a necessary condition for the formation of cross-hatched surface roughness patterns (Larson & Mateer, 1968). One of the experimental results adequately proved this requirement in the flow condition, which resulted in what was observed on a Lucite 55° half-angle cone as shown in Figure 2.3.

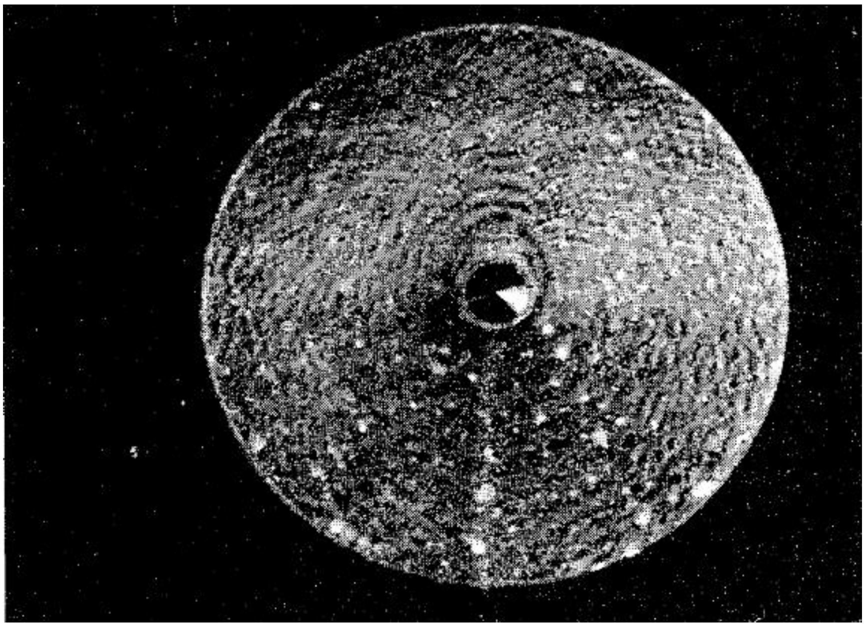

Figure 2.3: Lucite 55° half-angle cone tested at 5° angle of attack (Larson & Mateer, 1968)

They tested this cone at 5° angle of attack so that the cone will face two different local flow conditions, which were supersonic at its leeward side and subsonic at its windward side. As a result, the cross-hatched patterns were observed on the leeward side where the local flow was supersonic, but not noticed at all on the windward side thus proving this requirement in the flow conditions.

Laganelli and Nestler investigated the formation of surface roughness patterns on a steel-tipped wood wedge which comprised of three different types of woods: oak, maple and pine. The wedge was tested in NASA Langley High-Temperature Structures Tunnel with a Mach 7.4 flow in their experiment (Laganelli & Nestler, 1969). Figure 2.4 demonstrates the imprinted surface roughness patterns on the surface of every section of the wood wedge.

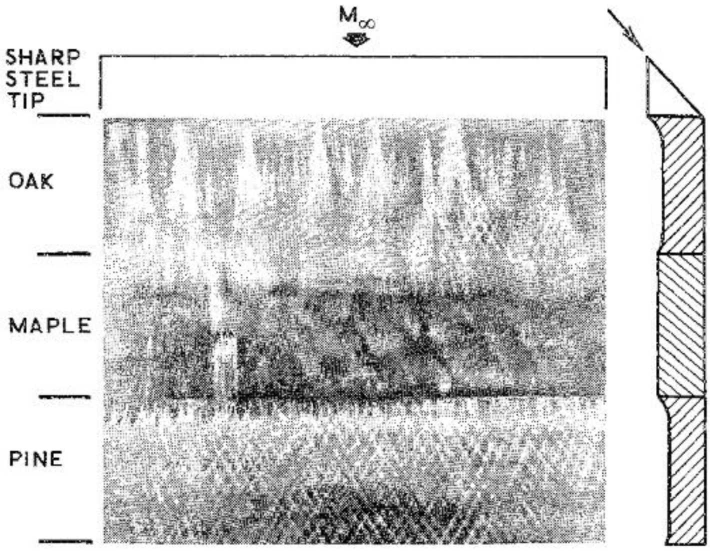

Figure 2.4: Surface patterns on wood (Laganelli & Nestler, 1969)

Several slender triangles were spotted at the oak section near the leading edge of the wood wedge as depicted in Figure 2.4. These slender triangles are called turbulent wedges, which are formed in one of the transition stages in the development of turbulence and is illustrated in Figure 2.5. Cross-hatched patterns were observed within the turbulent wedges, so the presence of transitional boundary layer was also a necessary factor. The maple section of the wedge was not imprinted with cross-hatched patterns possibly due to insufficient ablation (Laganelli & Nestler, 1969). The cross-hatched patterns were spotted again at the pine section without any turbulent wedges as the flow was already turbulent at there. Hence, turbulent boundary layer was also a necessary condition for the formation of cross-hatched surface roughness patterns.

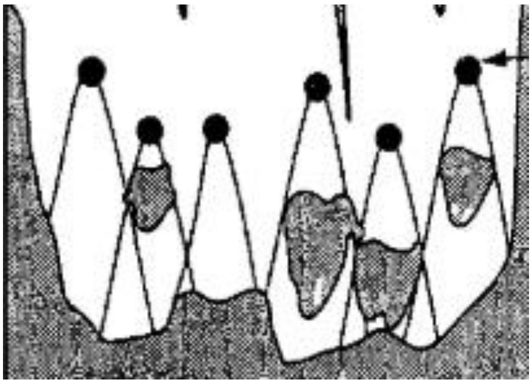

Figure 2.5: Schematic diagram of turbulent wedges (M.White, 2006)

As a summary from previous experimental studies, the necessary flow conditions for cross-hatched surface roughness patterns to form are a local supersonic flow, the presence of a transitional or turbulent boundary layer, and a sufficiently thin boundary layer.

T. C. Lin and Pu Qun discovered ablation patterns, their sequence of appearance, and their detailed surface striations in their research on the formation of regmaglypts on meteorites (Lin & Qun, 1987). Regmaglypts are the scalloped surface patterns which commonly appeared on the fusion crusts of the meteorites, as shown in Figure 2.6. This study is emphasized because the cross-hatched surface pattern is one of the sequences in the development of regmaglypt patterns. The physical mechanism on formation of regmaglypt is depicted in Figure 2.7.

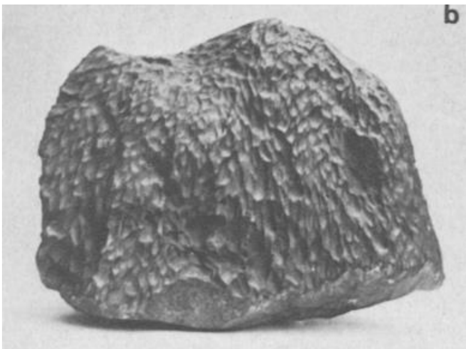

Figure 2.6: A meteorite with regmaglypts surface roughness pattern (Lin & Qun, 1987)

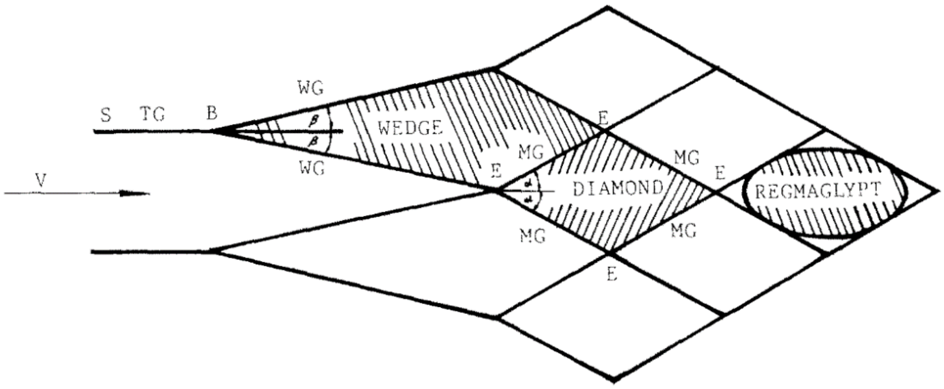

Figure 2.7: Schematic of formation of regmaglypt (Lin & Qun, 1987)

The mechanism starts with the streamwise trailing vortex, which is induced by a growing disturbance in the transitionary region of the boundary layer. This vortex grows and bifurcates into two vortices, which is named as wedge vortices and abbreviated as WG in Figure 2.7. Within a pair of wedge vortices, there is a turbulent wedge with a half-angle, ß. Eventually, the wedge vortices pair will intersect with the neighbouring pairs of wedge vortices. This intersection will induce a disturbance to the external supersonic flow and forms a conical Mach wave, which intersects with the turbulent boundary layer and generates a new pair of vortices, namely Mach vortices abbreviated as MG in Figure 2.7. The mechanism of generating Mach vortices cycles itself further downstream when the Mach vortices intersect and induce disturbance to the external supersonic flow.

Consequently, numerous pairs of Mach vortices are generated, the surface is ablated with their flow structures which are extremely hot, and finally diamond-shaped or cross-hatched surface roughness patterns are formed. Regmaglypt pattern is formed after the cross-hatched pattern and its respective flow mechanism will not be discussed due to regmaglypts being irrelevant to this research work.

2.2 The Onset of Turbulence and Corresponding Flow Behavior

Since cross-hatched patterns can only be formed in the transitional or turbulent boundary layer, the boundary layer transition process from laminar to turbulent is obligatory to understand. Frank M. White provided a comprehensive explanation on the corresponding topic. Figure 2.8 illustrates the top view and side view on the entire boundary layer transition process.

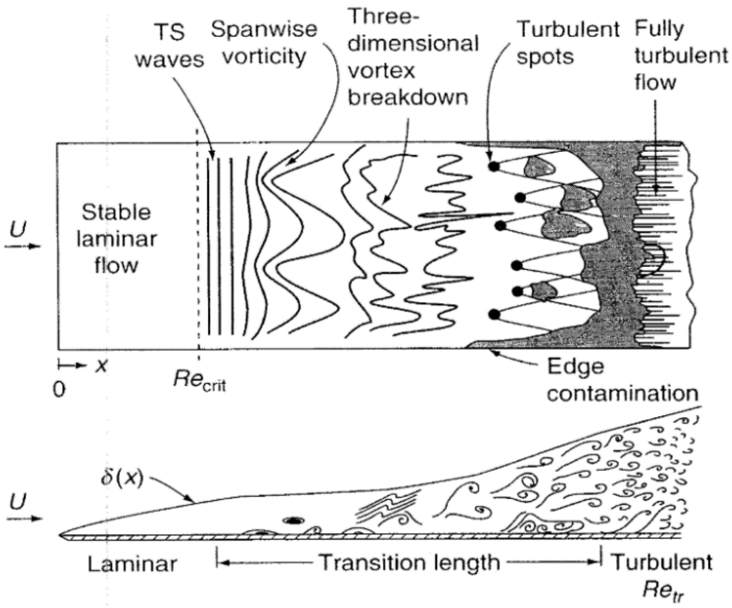

Figure 2.8: Natural boundary layer transition process (M.White, 2006)

The laminar flow losses its stability as it encounters infinitesimal disturbances and develops into the flow instability called Tollmien-Schlichting waves as abbreviated TS waves in Figure 2.8. Tollmien-Schlichting waves exhibits harmonic oscillation, and its amplitude increases gradually in streamwise direction. Velocity difference in the shear layer of Tollmien-Schlichting waves induce the formation of rotating spanwise vortices, which are named as Kelvin-Helmholtz vortices (Hu et al., 2019). After that, the difference of the spanwise travelling velocity of the wavy Kelvin-Helmholtz vortices deforms the vortices as the region with higher velocity will stretch the vortices longitudinally upfront relative to the slower one. This stage of the transition process is called spanwise vorticity. When the intensity of longitudinal stretching of the vortices is great enough, the spanwise deformed vortices will begin a cascading breakdown into smaller A-shaped vortices. Then, these vortices enter an intensely fluctuating state where the relevant frequencies and wave numbers approached randomness (M.White, 2006). At this stage, turbulent spots are observed and coalesce with each other to complete the transition process into fully turbulent flow. Note that the transition process depicted in Figure 2.8 occurs naturally when the boundary layer flow is quiet, and the wall is smooth. However, the transition process of boundary layer flow could be accelerated significantly for the rough wall.

X. Zhao and Q. Zhang investigated the Mach 5 boundary layer transition flow induced by distributed ramp shaped roughness elements experimentally and numerically to study the coherent structures in the corresponding boundary layer. They found out that the transition location of high speed boundary layer over roughness elements was much more upstream than the natural boundary layer case without roughness elements (Zhao & Zhang, 2018) as shown in Figure 2.9 and Figure 2.10.

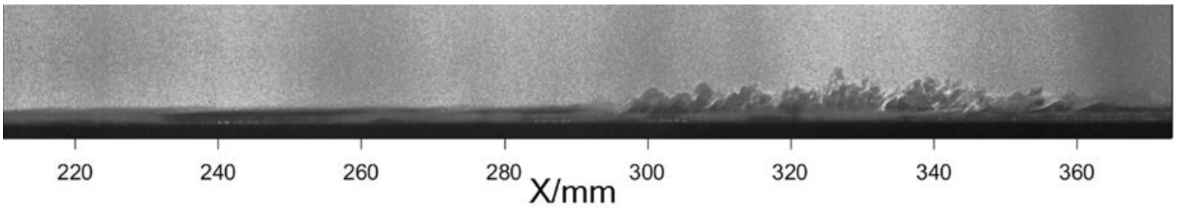

Figure 2.9: Visualization of the transition process over a flat plate surface (Zhao & Zhang, 2018)

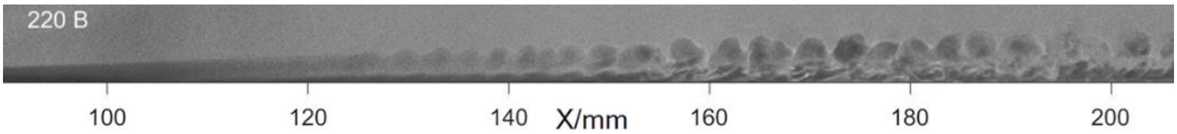

Figure 2.10: Visualization of the transition process over a surface with ramp roughness elements (Zhao & Zhang, 2018)

The roughness elements disturbed and accelerated the transition process by generating a pair of counter-rotating streamwise vortices, which was similar the one in the work of T. C. Lin and Pu Qun (Lin & Qun, 1987). This pair of vortices will then form a detached curved shear layer which make up the high vorticity areas and are highly unstable. These properties of the detached curved shear layer made it the main disturbance in the early transition stage until it breaks down. In the later transition stage, another high vorticity region with the main contribution in disturbing the boundary layer flow was the near wall boundary layer which was full of vortices, and these vortices were growing downstream due to higher wall friction (Zhao & Zhang, 2018).

2.3 Overview of Some Computational and Experimental Studies of Surface Roughness

2.3.1 Subsonic Flow Over Surface Roughness

The incompressible, turbulent boundary layer in subsonic flow had been studied experimentally by many researchers in the past over different kind of roughness topologies. This topic was studied by Nikuradse, who utilized sand grains cemented to the inner walls of pipes to simulate surface roughness in his experiment. This roughness topology was varied in roughness heights to investigate its effect on the subsonic flow. He discovered that the relative roughness of the wall has a dominant effect on the velocity distributions over the Reynolds number (Nikuradse, 1950).

Investigation on this topic was continued by Wu and Christensen. The roughness topology used in their experiment was recreated from a defaced turbine blade which was highly irregular and over a wide range of geometrical scales (Y. Wu & Christensen, 2007). Wu and Christensen studied the streamwise-wall-normal plane boundary layer over this roughness topology and a smooth wall for comparison purposes. In term of the inner-scaled mean velocity profiles, a downward shift was noticed for the rough wall relative to the smooth wall. However, the mean velocity profiles with velocity defect scaling matched with each other regardless of roughness topology.

The following experimental study was carried out by Mejia-Alvarez and Christensen, and the roughness model used in the previous experiment was inherited into their experiment. Their work was to study the impact of highly irregular walls derived from defaced turbine blade on a turbulent boundary layer under both developing and developed flow conditions (Mejia-Alvarez & Christensen, 2010). They uncovered that the scale of roughness effects (corresponding to mean velocity profiles in the previous study) was within the inner boundary layer for the developing flow condition, but the scale was growing as the flow develops until the whole boundary layer was affected.

On the aspect of numerical study on subsonic flows, S. Knotek and M. Jicha conducted CFD simulations of flow over a wavy surface to study the dependence of wall shear stress and pressure profile on the ratio of the wavelength to the wave amplitude, λ/A and air flow velocities, U (Knotek & Jícha, 2010, 2011). The air flow velocity defined in their simulations was very low, which between 0.5 m/s to 12 m/s. Therefore, the flow was incompressible and subsonic. They discovered the fluctuations of wall shear stress and pressure exhibited harmonic characteristic for $\lambda/A \geq 60$ and low values of U but the harmonic characteristic had deformed for shorter wavelengths and greater U. Shorter wavelengths tended to cause flow separation. They also found that the amplitudes of wall shear stress and pressure increase as the wavelength of wavy surface decreases. However, phase shift of the shear stress maximums decreases as the wavelength decreases. For velocities between 2 m/s to 12 m/s, the pressure minimums were found to be located between $\lambda/A = 40$ and $\lambda/A = 60$ (Knotek & Jícha, 2011).

2.3.2 Supersonic Flow Over Surface Roughness

The database of compressible flow over distributed surface roughness is much fewer than that of incompressible flow (Kocher et al., 2018). There was an experiment conducted by Ekoto et al. in a wind tunnel to investigate the supersonic turbulent boundary layer on 3-D surface roughness topologies with an incoming high-speed flow of Mach number = 2.86. Two surface roughness topologies were studied: square and diamond as depicted in Figure 2.11 (Ekoto et al., 2008).

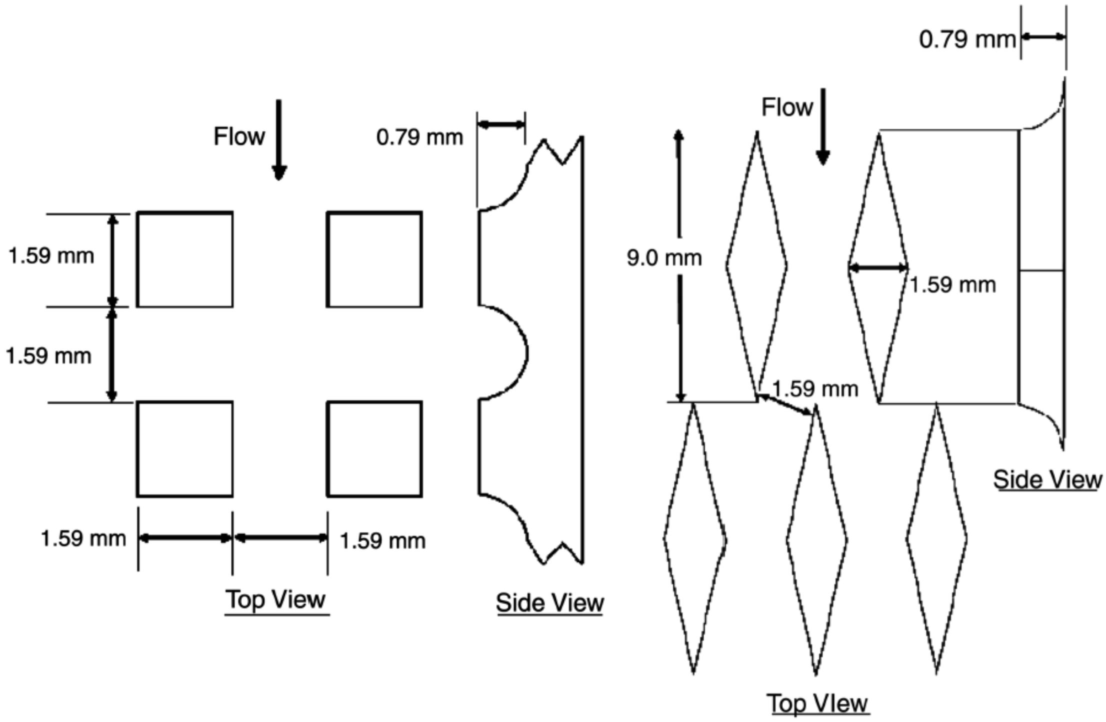

Figure 2.11: Square roughness topology (left) and diamond roughness topology (right) (Ekoto et al., 2008)

The results revealed the difference of the near-wall distortions on the square and diamond surface roughness, which can be described through pressure-sensitive paint (PSP) contours demonstrating the surface pressure distributions as illustrated in Figure 2.12. Note that the low-pressure region is indicated as a dark colour while the high-pressure region is indicated as a bright region in the PSP contours. The PSP contour for the square roughness model showed that the pressure distribution was oscillating with a relatively modest amplitude axially, in which the pressure in the channel was about 10% larger than that over the roughness-element surface (Ekoto et al., 2008). This observation means that the pressure difference over the square roughness model is relatively low and agrees with their expected flow structure on this model where only weak bow shocks are generated as illustrated in Figure 2.13.

Besides that, strong alternating axial bands of adverse and favourable pressure gradients was observed on the PSP contour for the diamond roughness model (Ekoto et al., 2008). The axial pressure distribution over diamond roughness model was oscillating with a greater amplitude than that over square roughness model. This flow condition favoured the formation of oblique shock waves and expansion waves, as constructed schematically within the PSP contour of diamond roughness model, where the pressure increases across the oblique shock wave while the pressure decreases across the expansion wave. This result agrees well with the experimental results of Bowersox and Latin, in which the shock waves and expansion waves were observed in the supersonic region of the boundary layer over their roughness topologies including sand-grain plates and uniformly machined plates (Latin & Bowersox, 2000).

To conclude, the localized flow distortions were stronger for the case of diamond roughness model as compared to that of square roughness model. Strong localized flow distortions could affect the mean and turbulent flow structure significantly, which means the turbulence in supersonic turbulent boundary layers could be altered by modifying the surface roughness topology (Ekoto et al., 2008).

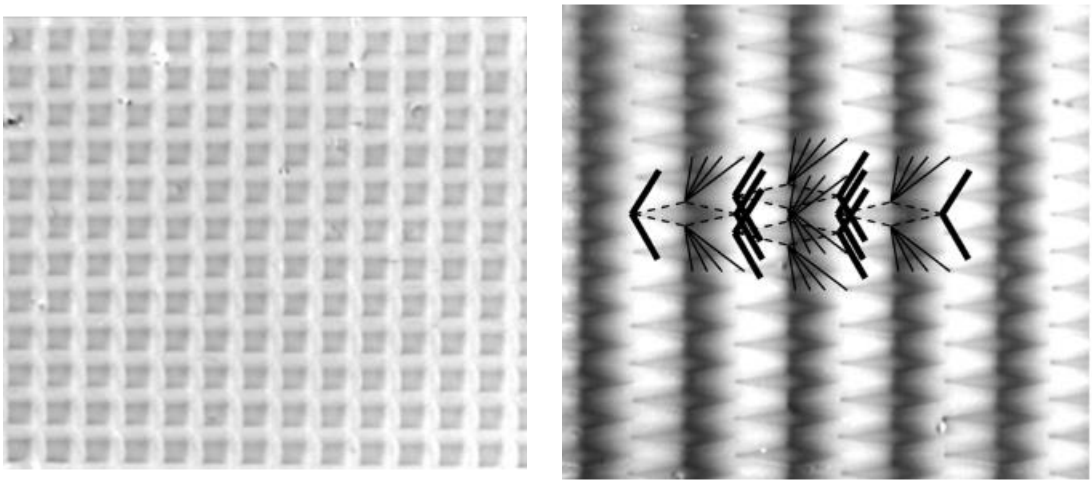

Figure 2.12: Surface pressure distributions for square roughness model (left) and diamond roughness model (right); flow is from left to right (Ekoto et al., 2008)

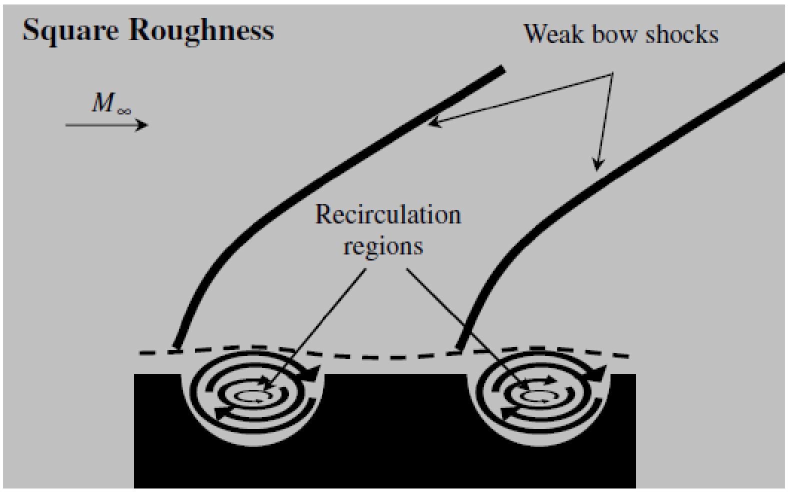

Figure 2.13: Schematic diagram of expected flow feature above the square roughness model (Ekoto et al., 2008)

Although the experimental results for compressible boundary layers discussed above are different with that for incompressible boundary layer, there is a similarity. The inner-scaled compressible boundary layer profiles of the rough wall were also having a downward shift as compared to the baseline smooth wall according to the experimental results of the three studies (Ekoto et al., 2009; Peltier et al., 2016; Sahoo et al., 2010).

C. J. Tyson and N. D. Sandham simulated supersonic fully developed turbulent flows over wavy surface using Direct Numerical Simulation (DNS) to investigate whether the mean flow and turbulence properties across the channel are significantly altered by the strong compressibility effects (Tyson & Sandham, 2013). The simulations were ran for three different Mach numbers: 0.3, 1.5 and 3.0 with amplitude-to-wavelength ratio ranging between 0.01 and 0.08. Note that only the results with Mach number 3.0 will be discussed as the Mach number simulated over the surface relief plate in the present research is 3.2. Increasing the wave's amplitude will have the following effects: the peak pressure value increases and shifts upwards (nearer to the surface peak), the flow separation region per wavelength becomes larger, and the percentage of pressure component in the total drag force increases. However, decreasing the wavelength will have the similar effects.

Van Pelt et al. defined three simplified roughness shapes representing a rocket nozzle's inner surface roughness as depicted in Figure 2.14: a forward facing-step (B), a cavity (C) and combination of a forward facing-step and a cavity (C). These simplified geometries were derived based on the full geometry of a nozzle inner surface roughness (A) and is varied in height from 6 to 46 percent of the boundary layer thickness (Van Pelt et al., 2014). They studied the effect of these surface roughness on the flow with free stream Mach number of 2 numerically and experimentally. Two flow parameters were evaluated in their research: drag and heat transfer. Their drag results are focused instead of heat transfer as the drag is the main physical quantity in the present research.

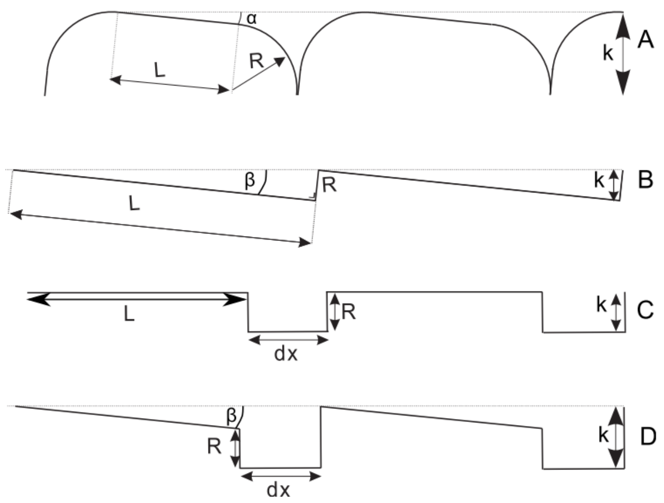

Figure 2.14: Baseline roughness geometry (A) and simplified roughness geometries (B, C, D) (Van Pelt et al., 2014)

They discovered that the drag coefficient of the cavity geometry is much smaller than the forward facing-step geometry due to the flow separation between the roughness elements. The gap between two roughness element tops is bridged by a shear layer (Van Pelt et al., 2014). Within the cavity, the flow circulates and losses its friction on the wall. This flow structure contributes to the smaller drag generated by the cavity geometry.

After the cavity geometry is combined with the forward facing-step geometry, the corresponding drag induced increases dramatically and transcends the drag induced by forward facing-step geometry slightly. This observation concludes that the forward-facing step has a dominant effect in inducing drag. As mentioned before, these geometries proposed by van Pelt et al. were simplified from complex rough-walled geometries of a rocket nozzle’s inner wall. In this research, the wavy surface derived from a doubly periodic function is studied as the wavy surface is a more realistic geometry representing the actual post-ablated nozzle's inner wall surface.

2.4 Computational Fluid Dynamics (CFD) Studies

The present research is conducted through numerical simulations with the utilization of a CFD software, which is ANSYS Fluent. Various turbulence models were introduced in the past to anticipate the effect of turbulence and were categorized as: Direct Numerical Simulation (DNS), Large Eddy Simulation (LES), and Reynolds-Averaged Navier Stokes (RANS). Correct selection of turbulence model is critical to solve the flow problem in this research accurately. Among the categories of turbulence models, DNS is not considered because DNS requires very high computational cost although DNS can provide the most accurate result and is capable of capturing the flow structures in detail (Zhao & Zhang, 2018). Besides DNS, the computational cost of LES is also quite high nowadays (Knotek & Jícha, 2012). Hence, RANS turbulence models are the ideal models to use for this case due to its low computational cost and high accuracy in solving turbulent flow.

Among the RANS turbulence models, k-ω SST model consists of two functions: standard k-ω model which solves the inner layer of the flow precisely and k-ε model which solves the outer layer of the flow, and performs well on both of these functions (Cunha Martins et al., 2019). Since this research requires the accurate solutions of both the inner and outer layer of the flow, k-ω SST model is chosen for the CFD simulations.

CHAPTER 3

METHODOLOGY

This chapter explains the procedures and setups for parametric numerical study in this research through three sections. The first section describes the pre-processing, which includes the processes such as geometry modelling, meshing, and defining boundary conditions. The second section elucidates the CFD simulation process in terms of the governing equations, selected turbulence model, and solution method and control. GIT is discussed under this section as well. Finally, the last section explains the selection of post-processing software and the types of results generated by using this software. Figure 3.1 illustrates the overall flow chart of this research work.

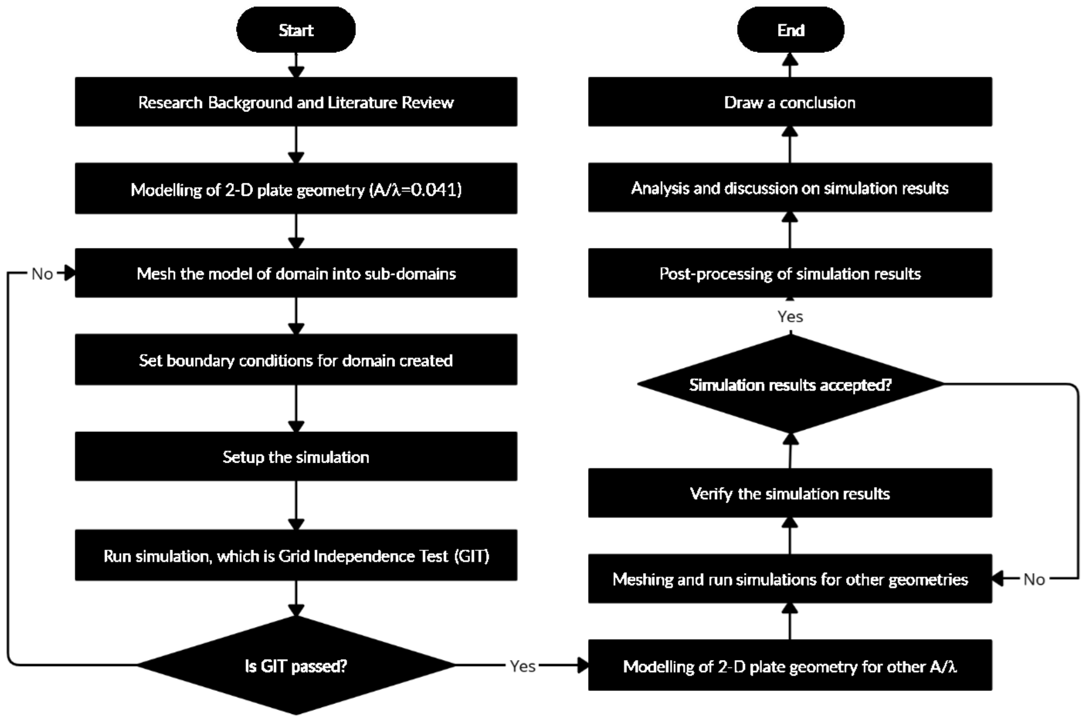

Figure 3.1: Overall flow chart of the current research work

3.1 Pre-processing

3.1.1 2-D Modelling of Nozzle

The CD nozzle functions to accelerate the gas flow in the nozzle to supersonic speed to generate thrust. The geometry of the CD nozzle is essential to model a fully developed turbulent flow condition for the relief plate. The profile of the flat nozzle is calculated by utilizing the geometry of an equivalent circular cross-sectional nozzle. The input parameters with known values, which are diameter of circular nozzle throat, d^* (10 mm), nozzle exit pressure, P_e (101,325 Pa), nozzle exit Mach number (3.2) and the diameter of circular nozzle exit, d_e (29 mm) are used to determine the profile of flat nozzle by applying Equation (3.1) to (3.4). By referring to the gas-dynamic property table for the specific heat ratio, γ =1.4, the specific flow rate, q, can be obtained for the desired value of Mach number through the interpolation method. The known q value will be used in Equation (3.1) to determine the cross-sectional area at the circular nozzle exit, A_e.

$$q(M^*) = \frac{A^*}{A_e} \tag{3.1}$$

The cross-sectional area at the throat of circular nozzle, A^*, is calculated using Equation (3.2) since $d^*$is already known.

$$A^* = \frac{\pi(d^*)^2}{4} \tag{3.2}$$

The calculated value of A_e is then substituted into Equation (3.3) together with the width of the plate, b, to determine the height of the flat nozzle exit, h_e. For the height of the flat nozzle throat, h^*, Equation (3.4) is applied.

$$h_e = \frac{A_e}{b} \tag{3.3}$$

$$h^* = \frac{A^*}{b} \tag{3.4}$$

With these equations above, the profile of the flat nozzle is determined. Then, the final geometry of the flat nozzle is modelled in SolidWorks, as illustrated in Figure 3.2, where the converging section is on the left side while the diverging section is on the right side. Note that the dimensions displayed in Figure 3.2 are all in mm.

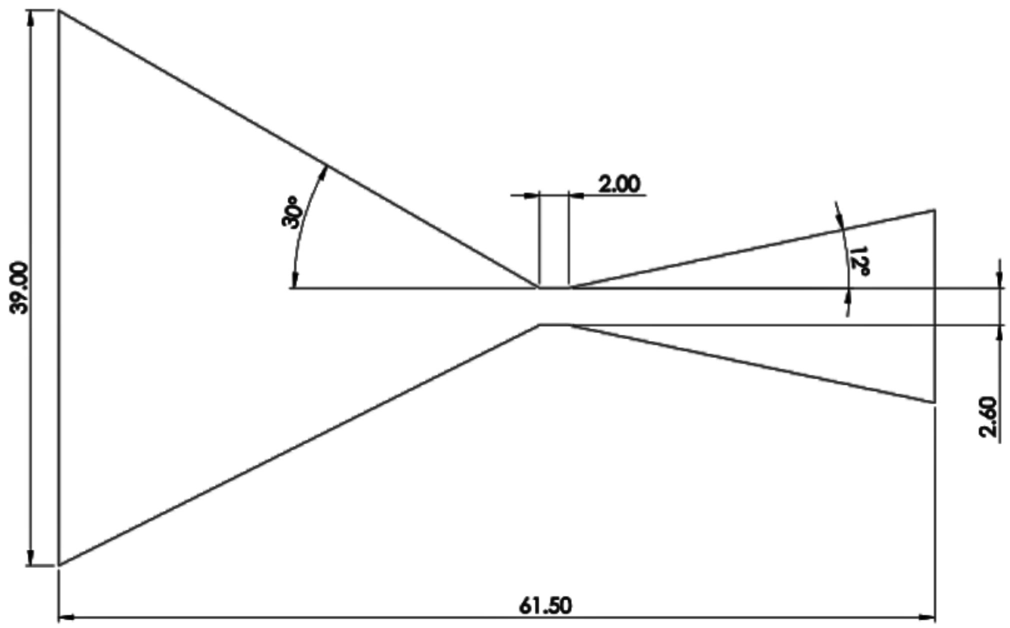

Figure 3.2: 2-D geometry of CD nozzle

3.1.2 2-D Modelling of Surface Relief Plate and Domain

SolidWorks is utilized for modelling 2-D plate geometry in this research work. The 2-D plate geometry follows the dimensions from H. Tan's work (Tan, 2020), where the plate model is 50 mm in length, 3 mm in thickness, 0.5 mm in the height of protrusion, and the sharp leading edge with an angle of 7°. Modification to his plate geometry is made, which is increasing the protrusion height by 50% to become 0.75 mm while maintaining the thickness of the plate.

Modelling of 2-D wavy surface on the relief plate requires a periodic function as expressed in Equation (3.5).

$$y = A\cos\left[\frac{2\pi x}{\lambda}\right] \tag{3.5}$$

where A and λ denote the amplitude and wavelength of the wavy surface respectively.

The manipulating variable in Equation (3.5) is λ, while A is constant for all the variants. The plate geometry is modelled for A/λ, ranging from 0.008 to 0.057. Figure 3.3 illustrates the 2-D relief plate with the wavy surface for $A/\lambda = 0.041$, and all the dimensions are in mm.

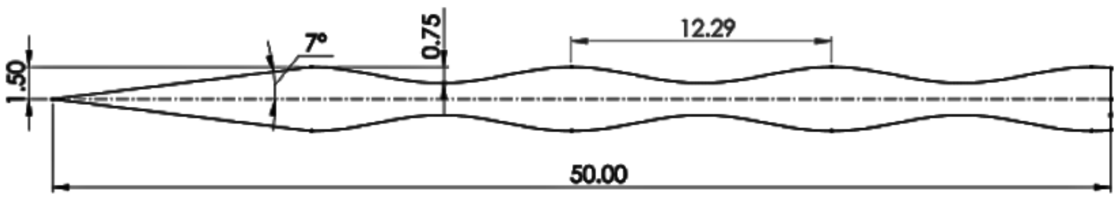

Figure 3.3: 2-D geometry of relief plate with the wavy surface for $A/\lambda = 0.041$